Automated Tire Footprint Segmentation

†Rodrigo Nava, ††Duc Fehr, ††Frank Petry, and †Thomas Tamisier

†*Luxembourg Institute of Science and Technology (LIST)*
Belvaux, Grand Duchy of Luxembourg
††*Goodyear Innovation Center Luxembourg*
Avenue Gordon Smith, Colmar-Berg, L-7750, Luxembourg

***Abstract*—Quantitative image-based analysis is a relatively new way to address challenges in automotive tribology. Its inclusion in tire-ground interaction research may provide innovative ideas for improvements in tire design and manufacturing processes. In this article we present a novel and robust technique for segmenting the area of contact between the tire and the ground. The segmentation is performed in an unsupervised fashion with Graph cuts. Then, superpixel adjacency is used to improve the boundaries. Finally, a rolling circle filter is applied to the segmentation to generate a mask that covers the area of contact. The procedure is carried out on a sequence of images captured in an automatic test machine. The estimated shape and total area of contact are built by averaging all the masks that have computed throughout the sequence. Since a ground-truth is not available, we also propose a comparative method to assess the performance of our proposal.**

***Index Terms*—Automotive tribology, Graph cuts, Ray feature error, Rolling circle filter, Superpixels, Tire footprint, Unsupervised segmentation.**

I. Introduction

The area of contact between the tire and the ground, commonly named tire footprint, plays an important role in tire performance. The shape and size depend on many factors such as characteristics of the road, tire inflation, and the forces applied to the tire. The aspect ratio of the tire footprint influences the driving characteristics of a vehicle. For instance, a low-aspect ratio (the tire footprint is short and wide) is very responsive to handling and traction. By contrast, a higher-aspect ratio (the tire footprint is long and narrow) allows drivers to handle in a more predictable manner [1].

A common way to capture a tire footprint is through the use of an automatic test machine (ATM). In an ATM, a tire rolls on a glass plate while its movement is recorded using a high-speed camera. The images are acquired in grayscale and the darkest levels depict the tire footprint (see Figure 1).

Inspection of a tire footprint is a time consuming task. There have been some efforts to automate it. In [2]–[4], the tire footprint segmentation is based on a thresholding method, (e.g. Otsu [5]); while in [6], a combination of a thresholding method and wavelets is proposed. However, due to changes in lighting conditions and acquisition, a thresholding method is not always robust enough to segment the tire footprint properly.

A more sophisticated solution is presented in [7] where the authors use level sets [8] to segment the tire footprint. The limitation is that the level set needs an initial mask, if the initialization is not close to the observed tire footprint, the method may lead to a mis-segmentation.

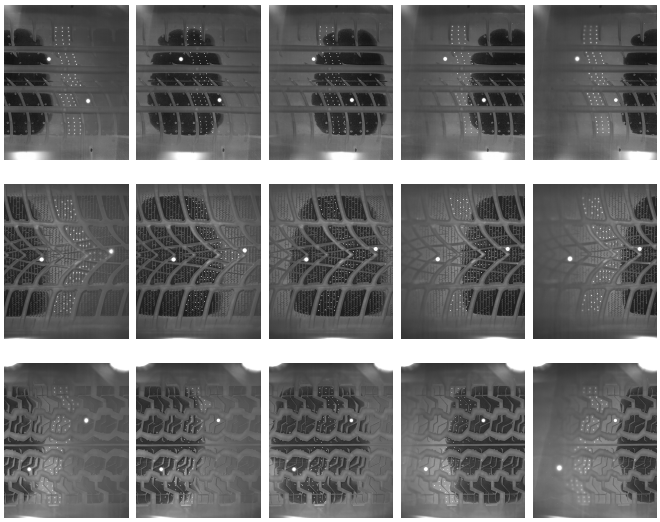

Figure 1. Three tire footprint sequences captured in an automatic test machine. A tire rolls under free conditions from right to left on a glass plate while its movement is captured with a high-speed camera. The darkest area depicts the tire footprint. Only those frames where the footprint is shown full size are considered for segmentation. Note that the non-uniform illumination changes the appearance of the contact area throughout the sequence.

The shape of a tire footprint has a major impact in the process of designing a tire. Therefore, many studies that have addressed the topic remain proprietary. On the other hand, in many cases, the shape of the tire footprint is assumed rectangular [9]. As a consequence, very little literature devoted to the analysis and segmentation of the tire footprint exists.

The problem addressed here represents a challenging task. In a given image, only a small area of the tire is in contact with the ground. The main drawback is that both the non-contact area and contact area possess very similar intensity values.

Our main contribution is a novel technique for the automated segmentation of the tire footprint in an unsupervised fashion. This technique allows analyzing the shape of the tire footprint and computing total and effective areas of contact. Also a new method to compare different segmentation results without ground-truth is introduced in the paper.

ISBN 978-90-827970-1-5

II. Methodology

The methodology presented in our study is composed of several stages. First, in order to minimize the effects of the illumination, an estimation of the background is calculated and subtracted. An over-segmentation is computed with superpixels that are then clustered using Graph cuts [10]–[12]. Since the clustering sometimes does not group superpixels lying at the boundaries of the tire footprint properly, we include an improvement to alleviate this issue. Finally, a mask that covers the tire footprint is obtained with a rolling circle filter.

A. Illumination compensation

The first step is to minimize the effects of the non-uniform illumination. As [13] pointed out, a retrospective method relies on the current data to estimate an intensity model that can be used to correct uneven illumination. Although there are many variants, we use the following formulation:

$$g\left(x,y\right) = f\left(x,y\right) - h\left(x,y\right) + K \tag{1}$$

where $f(x,y)$ is the intensity image, $h(x,y)$ is the estimated illumination model and K is a constant that preserves luminance. A common way to estimate $h(x,y)$ is using a low-pass version of $f(x,y)$. We take advantage of the image sequence $\mathcal{S}$ and compute an average image as follows: $h(x,y) = \frac{1}{M}\sum_{i=1}^{M} f_i(x,y)$ where $f_i(x,y) \in \mathcal{S}$ and M is the number of images in the sequence.

B. Superpixel partition

In order to include spatial connectivity information, an initial partition $\mathcal{P}$ of superpixels is generated using simple linear iterative clustering (SLIC) [14].

SLIC seeds n centroids $\{C_j | j = 1, \ldots, n\}$ on a regular grid in the image plane and clusters pixels using k-means. SLIC measures the affinity of the pixels with the nearest centroids based on their intensity and spatial information. The distance is calculated as $D = \sqrt{d_c^2 + (\frac{m^2}{N^2})d_s^2}$.

In this case, d_c is the Euclidean distance between the intensities of the pixel i and the centroid C_j and d_s is the Euclidean distance between the pixel i and the centroid C_j measured in pixels. N is the size of the superpixel and m is a regularization parameter that controls superpixel compactness. In our case, we use the relationship $n = \frac{H*W}{N^2}$ where H and W are the height and width of the image, respectively. In our experiments, we use $m = 10$ and $N = 10$ (see Figure 2).

C. Feature extraction

A feature descriptor $\boldsymbol{x}_p$ is built for each superpixel p in the partition $\mathcal{P}$ as follows:

$$\boldsymbol{x}_p = [\mu_p,\, \max_p,\, \min_p,\, \text{posx}_p,\, G_{p,\sigma_i}] \tag{2}$$

where μ_p is the mean intensity value, and $\max_p$ and $\min_p$ are the maximum and minimum intensity values within the selected superpixel p, respectively. posx_p is the normalized position of the centroid of the superpixel p measured on the X-axis.

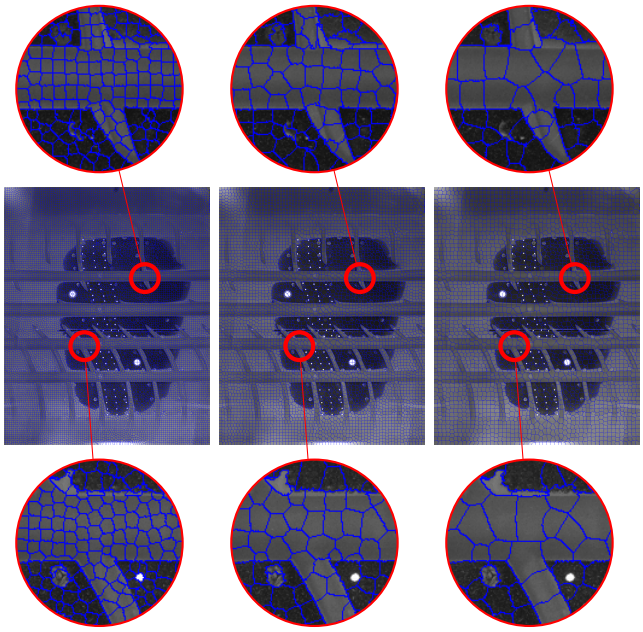

(a) (b) (c)

Figure 2. Over-segmentation with SLIC superpixels. The red circles show the magnified region. (a) $N = 10$, (b) $N = 15$, and (c) $N = 20$.

Since, the intensity and spatial features are not sufficient for an accurate segmentation, then we include features based on multi-scale filtering.

$$G_{p,\sigma_i} = \text{mean}\left\{ g\left(x,y\right) * e^{-\frac{(x^2+y^2)}{2\sigma_i^2}}\Big|_p \right\} \tag{3}$$

G_{p,σ_i} is the mean value of the response to the convolution of the corrected image $g(x,y)$ with the Gaussian filter $e^{(\bullet)}$ within the superpixel p. The symbol $*$ represents the convolution and $\sigma_i = \sqrt{1.5}^i$ with $i = \{0, \ldots, 7\}$.

In summary, a feature descriptor $\boldsymbol{x}_p$ is a combination of first-order intensity statistics, spatial information, and filter responses which resemble texture characteristics.

All of these features are concatenated one after another to build a 12-length vector that describes the superpixel p.

D. Clustering

In order to segment the tire footprint, the superpixel partition $\mathcal{P}$ is used as a graph. Every superpixel represents a node and the neighboring superpixels are connected via the Euclidean distance between the feature descriptors described in Eq. (2).

Graph cut based methods are a powerful and suitable tool for segmentation in n-D images [15]. They find the optimal segmentation with respect to an objective function that contains two terms: region-based and boundary term. The former evaluates the penalty for assigning a superpixel to a given region, while the latter evaluates the penalty for assigning two neighboring superpixels to two different partitions.

ISBN 978-90-827970-1-5 © EURASIP 2018

Due to the fact that Graph cuts need hard constraints as initialization, namely, samples that belong to the object to be segmented and samples that belong to the background; then, we use a Gaussian mixture model [16] to estimate the probability distribution of the tire footprint features and the different background features. We assume the distribution of each class is normal $p(\boldsymbol{x}) = \sum_{i=1}^{K} \tilde{\phi}_i \mathcal{N}(\tilde{\mu}_i, \tilde{\sigma}_i)$. The parameters $\tilde{\phi}_i$, $\tilde{\mu}_i$, and $\tilde{\sigma}_i$ are estimated using the expectation-maximization algorithm.

We found experimentally that the optimal number of classes is four: contact area ($cl = 1$), slip area ($cl = 2$), non-contact area ($cl = 3$), and control marks ($cl = 4$). cl represents the label of the class.

E. Boundary refinement

When a tire rolls under the effects of a power transmission or braking, local forces cause a deformation of the rubber and generate a partial slide or tangential displacement within the contact area. Such a displacement is known as slip region and is considered part of the tire footprint in this paper.

Due to the smooth transition between the non-contact area and the slip region, it is not clear where the segmentation should be stopped. The affinity between the contact area and the slip region leads Graph cuts to fail in reaching the boundary of the tire footprint. Hence, we include a refinement to alleviate this issue and recover more precise boundaries as follows:

- A list $\mathcal{L}$ of superpixels labeled as $cl = 1$ that lie on the border of the tire footprint is built.
- A second list $\mathcal{E}$ of superpixels labeled as $cl = 2$ is also built.

We define superpixel adjacency as: Let $x \in \mathcal{L}$ and $y \in \mathcal{E}$ be two superpixels. We say that x and y are adjacent superpixels, if they are 8-neighbors.

For each superpixel $x \in \mathcal{L}$, the Euclidean distance between x and its adjacent superpixels $y \in \mathcal{E}$ is calculated. If the Euclidean distance $d(x, y) \leq k_d * d(\mu_j, y)$ where $\{j = 3, 4\}$, μ_j is the estimated centroid of the class j, and k_d is a scaling factor. Then, the label of the superpixel y is updated to $cl = 1$. It means the border of the tire footprint grows. Otherwise, it remains unchanged (see Figure 3).

This is an iterative method that stops when there are no more updated labels. The scaling factor $k_d = 0.6$ was determined experimentally.

F. Rolling circle filter

The total area (TA) of contact is defined as the elliptical contact area between the tire and the surface without considering any grooves [17].

Since not all the TAs are convex, it is not possible to construct a convex hull.

Inspired by [3], we designed a rolling circle filter to compute a mask K that covers the segmented tire footprint. The algorithm uses a circle that rolls around the segmented tire footprint to calculate the contact points.

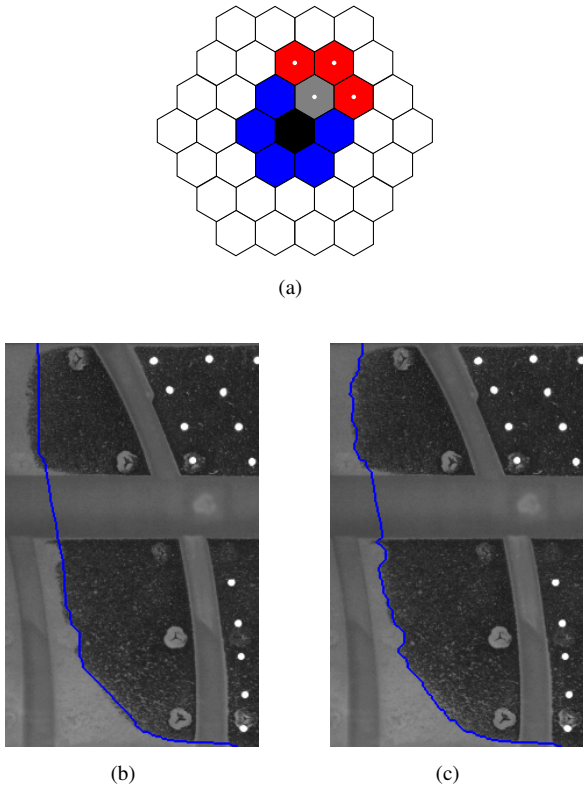

(a) (b) (c)

Figure 3. Boundary refinement. (a) The hexagons represent superpixels in an image. The black hexagon is the tire footprint, blue and gray hexagons depict the boundary. The labels of the adjacent superpixels $y \in \mathcal{E}$ (red) are updated to $cl = 1$, if their corresponding distances to the superpixel $x \in \mathcal{L}$ (gray) is less than their distances to any other centroid μ_j. Curve (b) before and (c) after the refinement.

The implementation of the rolling circle filter is made by convolving a circle template with the segmented tire footprint. Then, the contact points are linked with a B-spline in order to build the mask K that covers the TA (see Figure 4).

III. Performance comparison without reference

One of the contributions in this article is a novel method to compare the segmentation performance of our proposal if a ground-truth is not available.

When a tire is rolling, the footprint varies to some extend. This variation is introduced on purpose to alleviate tire noise issues. Therefore, it is not possible to define a ground truth. However, the variations of the size and shape do not change dramatically. Under this assumption, we consider that the shape and total area remain almost constant throughout the image sequence; then, it is possible to define a quality of segmentation.

- A family of masks $\{K_i | i = 1, \ldots, M\}$ that covers the TAs is calculated independently throughout the image sequence $\mathcal{S}$, see Figure 5(a).
- These masks are aligned using an affine transformation $f : K \rightarrow B$ (see Figure 5(b)). We consider the mask with the minimum eccentricity $K_\epsilon = \min_\epsilon\{K_i\}$ as the reference for the alignment.

ISBN 978-90-827970-1-5 © EURASIP 2018

Table I
COMPARISON PERFORMANCE OF OUR PROPOSAL, GAUSSIAN MIXTURE MODEL, AND K-MEANS++ . FIVE IMAGE SEQUENCES WERE USED TO TEST THE METHODS. WE SHOW THE AVERAGE ERROR MEASURED BETWEEN THE MEAN SHAPE K_μ AND THE MASKS K_i. RFE IS A NORMALIZED METRIC BETWEEN $[0, 1)$ WHERE 0 IS THE BEST MARK. DI IS ALSO A NORMALIZED METRIC BETWEEN $[0, 1]$ WHERE 1 IS THE BEST SCORE. BOLD VALUES REPRESENT THE BEST RESULTS.

	Ray feature error (RFE) [18]			**Dice index (DI)** [19]		
	GMM	*KM++*	*Our proposal*	*GMM*	*KM++*	*Our proposal*
Im. Seq. #1	0.0086	0.0412	**0.0078**	0.9843	0.9233	**0.9861**
Im. Seq. #2	0.0059	0.0318	**0.0052**	0.9896	0.9429	**0.9907**
Im. Seq. #3	0.0246	0.0204	**0.0097**	0.9474	0.9609	**0.9825**
Im. Seq. #4	0.0175	0.0283	**0.0097**	0.9664	0.9551	**0.9826**
Im. Seq. #5	**0.0046**	0.0199	0.0047	**0.9916**	0.9615	**0.9916**

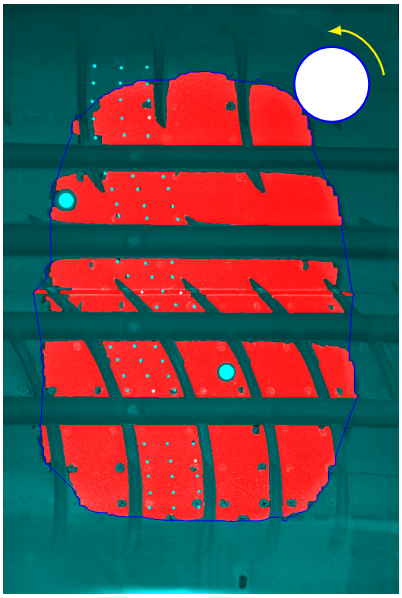

Figure 4. Rolling circle filter. A circle template rolls around a segmented tire footprint (red) to calculate contact points (blue line) and build a mask that covers the total area of contact.

- A statistic model described by the mean shape K_μ and the first eigenvalues $K_{-\lambda}$ and $K_{+\lambda}$ is built.

K_μ is considered as the ground-truth of the sequence $\mathcal{S}$ (see Figure 5(c)). Therefore, it is possible to evaluate the segmentation error between K_μ and all K_i. Here, we use two metrics: Ray feature error (RFE) [18] and Dice index (DI) [19]. RFE is a normalized metric between $[0, 1)$ where 0 is the best mark. DI is also a normalized metric between $[0, 1]$ where 1 is the best score.

IV. MATERIALS & EXPERIMENTS

In order to validate our proposal, five image sequences were recorded on the ATM. The sequences include summer and winter tires and were capture under free rolling conditions. For each sequence, 15 frames of size 1024×1280 were extracted at different times while the tires were rolling from right to left and saved as grayscale images. The segmentation performance was evaluated between the mean total area K_μ and the 15 masks K_i that correspond to the same sequence.

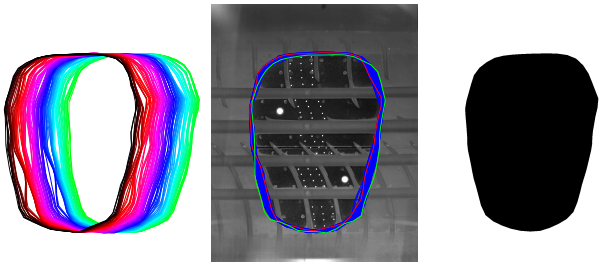

(a) (b) (c)

Figure 5. Generation of the ground-truth. (a) The masks K_i are calculated throughout the image sequence $\mathcal{S}$. (b) K_i are aligned and the mean shape K_μ and first eigenvalues $K_{-\lambda}$ (green) and $K_{+\lambda}$ (red) are computed. The image shows the aligned masks over a tire footprint. (c) K_μ is used as the ground-truth of the sequence $\mathcal{S}$.

For RFE, the sample points were collected every $30°$. We also conducted experiments with unsupervised clustering using two standard methods: Gaussian mixture models (GMM) [16] and K-means++ (KM++) [20]. For each of them, we chose experimentally the best parameters in terms of Dice index and Ray feature error. The comparison between the standard methods and our proposal is summarized in Table I.

V. CONCLUSIONS

We presented a novel and robust technique that allows analyzing the shape of a tire footprint captured in an automatic test machine under free rolling conditions. The main difficulty is the non-uniform illumination. Thus, we included a pre-processing step that estimates the background and minimizes the effects of the lighting conditions. However, further research need to be done to improve background estimation because in some cases an adjustment of the parameters is needed due to the changes in the color of the rubber. Also, the inclusion of superpixels improved the coherence of the segmentation.

It is well-known that unsupervised methods are not as powerful as supervised methods. However, the methodology presented here generates a very close estimation of the real tire footprint. Our proposal outperformed the results obtained with standard clustering methods such as GMM and KM++. Since the technique does not assume any *a priori* knowledge of the image, it is possible to extend its application to other fields or modalities.

ISBN 978-90-827970-1-5

REFERENCES

[1] A. Kapoor, S. C. Tung, S. E. Schwartz, M. Priest, and R. S. Dwyer-Joyce, "Automotive Tribology," in *Modern Tribology Handbook Vol. 2*, B. Bhushan, Ed., chapter 32, pp. 1187–1229. CRC Press, 2001.

[2] K. Jankowska, T. Krzyzynski, and A. Domscheit, "Vision-based analysis of the tire footprint shape," in *Computer Vision and Graphics: International Conference*, K. Wojciechowski, B. Smolka, H. Palus, R. S. Kozera, W. Skarbek, and L. Noakes, Eds., 2006, vol. 32.

[3] R. S. Lu, N. Liu, and X. H. Chen, "Measurement of vehicle tire footprint pattern and pressure distribution using piezoresistive force sensor mat and image analysis," in *Measurement Technology and Intelligent Instruments IX*, 2010-09, vol. 437, pp. 467–471.

[4] C. Zhang and Y. h. Cheng, "A quadric image segmentation for the feature extraction of tire surface wear," in *6th International Conference on Intelligent Systems Design and Applications*, 2006, vol. 2, pp. 457–462.

[5] Nobuyuki Otsu, "A threshold selection method from gray-level histograms," *Automatica*, vol. 11, no. 285-296, pp. 23–27, 1975.

[6] C. Zhang and Y. h. Cheng, "A hybrid template match approach based on wavelet analysis and threshold segmentation for detecting tire surface wear," in *IEEE International Conference on Control and Automation*, 2007, pp. 1079–1084.

[7] W. Zhen, W. Yunpeng, and L. Shiwu, "Tire impressions image segmentation algorithm based on C-V model without re-initialization," in *IEEE 3rd International Conference on Communication Software and Networks*, 2011, pp. 541–545.

[8] T. F. Chan and L. A. Vese, "Active contours without edges," *IEEE Transactions on Image Processing*, vol. 10, no. 2, pp. 266–277, 2001.

[9] V. Ivanov, K. Augsburg, and B. N. Shirokov, "Evaluation of tire contact properties using nondestructive testing. part 2: Experimental determination and fuzzy model of the contact parch in the static state," *Journal of Friction and Wear*, vol. 29, no. 6, pp. 448–454, 2008.

[10] Y. Boykov, O. Veksler, and R. Zabih, "Efficient approximate energy minimization via graph cuts," *IEEE transactions on Pattern Analysis and Machine Intelligence*, vol. 20, no. 12, pp. 1222–1239, 2001.

[11] Y. Boykov and V. Kolmogorov, "An experimental comparison of min-cut/max-flow algorithms for energy minimization in vision.," *IEEE transactions on Pattern Analysis and Machine Intelligence*, vol. 26, no. 9, pp. 1124–1137, 2004.

[12] V. Kolmogorov and R. Zabih, "What energy functions can be minimized via graph cuts?," *IEEE transactions on Pattern Analysis and Machine Intelligence*, vol. 26, no. 2, pp. 147–159, February 2004.

[13] K. Smith, Y. Li, F. Piccinini, G. Csucs, C. Balazs, A. Bevilacqua, and P. Horvath, "CIDRE: an illumination-correction method for optical microscopy," *Nature Methods*, vol. 12, no. 5, pp. 404–406, 2015.

[14] R. Achanta, A. Shaji, K. Smith, A. Lucchi, P. Fua, and S. Süsstrunk, "SLIC superpixels compared to state-of-the-art superpixel methods," *IEEE Transactions on Pattern Analysis and Machine Intelligence*, vol. 34, no. 11, pp. 2274–2282, 2012.

[15] S. Bagon, "Matlab wrapper for graph cut," http://www.wisdom.weizmann.ac.il/~bagon, December 2006.

[16] G. J. McLachlan and D. Peel, *Finite mixture models*, Wiley Series in Probability and Statistics, New York, 2000.

[17] R. Muniandy, D. Moazami, H. Hamid, and S. Hassim, "Characterization of effective tire contact area for various tread patterns," *Instrumentation Science & Technology*, vol. 42, no. 1, pp. 15–26, 2014.

[18] J. Olveres, R. Nava, B. Escalante-Ramírez, E. Vallejo, and J. Kybic, "Left ventricle Hermite-based segmentation," *Computers in Biology and Medicine*, vol. 87, pp. 236–249, 2017.

[19] L. R. Dice, "Measures of the amount of ecologic association between species," *Ecology*, vol. 26, no. 3, pp. 297–302, 1945.

[20] D. Arthur and S. Vassilvitskii, "K-means++: The advantages of careful seeding," in *Proceedings of the Eighteenth Annual ACM-SIAM Symposium on Discrete Algorithms*, 2007, pp. 1027–1035.

ISBN 978-90-827970-1-5